Journal of Biomolecular NMR, 5 (1995) 233–244
ESCOM

J-Bio NMR 247

Internal motions of apo-neocarzinostatin as studied by ^{13}C NMR methine relaxation at natural abundance

Joël Mispelter*, Claudine Lefèvre, Élisabeth Adjadj, Éric Quiniou and Vincent Favaudon

INSERM U350, Institut Curie, Biologie, Centre Universitaire, Bât 112, F-91405 Orsay Cedex, France

Received 30 August 1994
Accepted 19 October 1994

Keywords: Neocarzinostatin; Backbone dynamics; Side-chain dynamics; ^{13}C NMR relaxation

Summary

Dynamics of the backbone and some side chains of apo-neocarzinostatin, a 10.7 kDa carrier protein, have been studied from ^{13}C relaxation rates R1, R2 and steady-state ^{13}C-{^1H} NOEs, measured at natural abundance. Relaxation data were obtained for 79 nonoverlapping C^α resonances and for 11 threonine C^β single resonances. Except for three C^α relaxation rates, all data were analysed from a simple two-parameter spectral density function using the model-free approach of Lipari and Szabo. The corresponding C-H fragments exhibit fast ($\tau_e < 40$ ps) restricted libration motions ($S^2 = 0.73$ to 0.95). Global examination of the microdynamical parameters S^2 and τ_e along the amino acid sequence gives no immediate correlation with structural elements. However, different trends for the three loops involved in the binding site are revealed. The β-ribbon comprising residues 37 to 47 is spatially restricted, with relatively large τ_e values in its hairpin region. The other β-ribbon (residues 72 to 87) and the large disordered loop ranging between residues 97–107 experience small-amplitude motions on a much faster (picosecond) time scale. The two N-terminal residues, Ala^1 and Ala^2, and the C-terminal residue Asn^{113}, exhibit an additional slow motion on a subnanosecond time scale (400–500 ps). Similarly, the relaxation data for eight threonine side-chain C^β must be interpreted in terms of a three-parameter spectral density function. They exhibit slower motions, on the nanosecond time scale (500–3000 ps). Three threonine (Thr^{65}, Thr^{68}, Thr^{81}) side chains do not display a slow component, but an exchange contribution to the observed transverse relaxation rate R2 could not be excluded at these sites. The microdynamical parameters (S^2, τ_e and $R2_{ex}$) or (S^2_{slow}, S^2_{fast} and τ_{slow}) were obtained from a straightforward solution of the equations describing the relaxation data. They were calculated assuming an overall isotropic rotational correlation time τ_c for the protein of 5.7 ns, determined using standard procedures from R2/R1 ratios. However, it is shown that the product $(1 - S^2) \times \tau_e$ is nearly independent of τ_c for residues not exhibiting slow motions on the nanosecond time scale. In addition, this parameter very closely follows the heteronuclear NOEs, which therefore could be good indices for local fast motions on the picosecond time scale.

Introduction

Understanding the implications of protein structure and dynamics for their biological activity has become a subject of intensive studies (Schulz and Schirmer, 1978; McCammon and Harvey, 1987). In particular, internal motions may be related to protein–ligand binding, regulation of enzymatic activity and cooperative effects (Careri et al., 1975; Ringe and Petsko, 1985; Frauenfelder et al., 1991). They include low-amplitude subpicosecond or picosecond fluctuations of individual atoms, collective local or rigid-body movements on a longer time scale (10^{-12} to 10^{-3} s) and triggered conformational changes (10^{-9} to 10^3 s) (Karplus, 1986).

NMR is a unique technique, able to probe local mobility on a per residue basis for proteins in solution (Wagner and Wüthrich, 1986). Particularly, heteronuclear NMR spin relaxation provides quantitative information about the overall rotational diffusion of the protein and about internal motions with similar or faster rates (10^{-12} to 10^{-9} s). In addition, some information about slow conformational exchange (10^{-6} to 10^{-3} s) may be inferred from transverse relaxation times T2 (Palmer et al., 1991; Powers et al., 1992; Fushman et al., 1994; Orekhov et al.,

*To whom correspondence should be addressed.

1994) or relaxation times in the rotating frame T1ρ (Deverell et al., 1970; Blackledge et al., 1993; Szyperski et al., 1993). Pioneering studies on ^{15}N or ^{13}C species were based on 1D schemes with direct observation of the heteronuclei. The low resolution and sensitivity of these methods have been drastically improved by the use of two-dimensional inverse experiments (Sklenář et al., 1987; Nirmala and Wagner, 1988), which are, moreover, increasingly performed on isotopically enriched proteins. Almost all the present studies deal with ^{15}N nuclei instead of ^{13}C (Wagner, 1993). To our knowledge, extensive ^{13}C relaxation measurements have so far been carried out only on few relatively small proteins or peptides of MW ≤ 6.5 kDa, at natural abundance (Ribeiro et al., 1980; Nirmala and Wagner, 1988; Dellwo and Wand, 1989; Palmer et al., 1991,1993; Kelsh et al., 1992; Arvidsson et al., 1994). This is due in part to the much higher cost of ^{13}C labelling, although this technique is potentially more informative than ^{15}N NMR because it samples both main- and side-chain internal motions. In contrast, ^{15}N relaxation measurements are mainly restricted to amide groups. Nevertheless, specific labelling has been used for small (Daragan et al., 1993; Lepre et al., 1993) and large (Nicholson et al., 1992; Kemple et al., 1994) proteins.

We report here an analysis of natural abundance ^{13}C longitudinal and transverse relaxation rates, and ^{13}C-{^1H} steady-state NOE values for most alpha-methine carbons of apo-neocarzinostatin, and for 11 threonine beta-methine carbons resonating within the same spectral range. The native protein (10.7 kDa, 113 amino acids) binds a

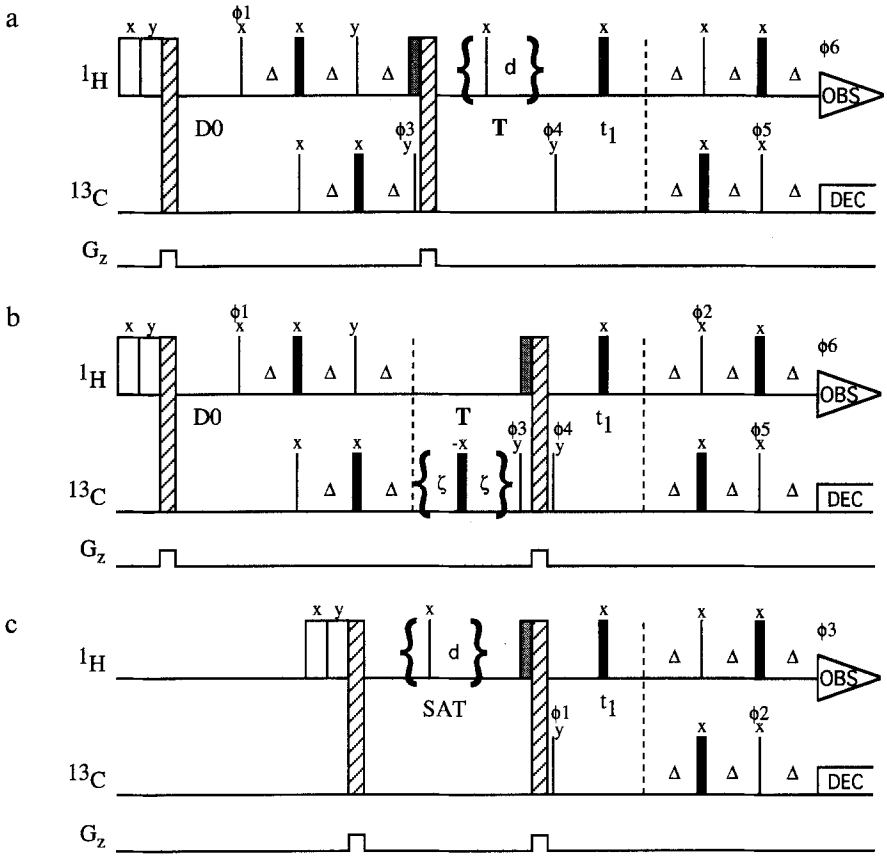

Fig. 1. Pulse sequences for measurement of the relaxation parameters R1, R2 and NOE for backbone methine carbons. The pulse sequences shown were used to derive (a) R1; (b) R2; and (c) heteronuclear steady-state NOEs. Thin and thick vertical bars represent 90° and 180° pulses, respectively. A stippled bar represents a 3 ms purge pulse, and hatched bars indicate homogeneity spoiling z-gradient pulses (0.2 T/m) applied during 8 ms (first gradient) or 0.5 ms (second gradient). After each z-gradient pulse, a 3 ms delay allows recovery of magnetic field homogeneity. White bars correspond to spin-lock pulses, applied during 1 ms along x or y. The delay Δ is set to 3.3 ms, which is slightly less than the mean $1/2J_{CH}$, in order to minimize relaxation losses. The spin-echo delay ζ is taken equal to 0.25 ms. During the periods T and SAT (4 s) in the T1 and NOE experiments, respectively, ^1H saturation is performed by means of 90° pulses spaced 7 ms apart. Preparation periods D0 are equal to 2.5 s (sequence a) or 1.8 s (sequence b). Relaxation delays T are incremented from one T1 or T2 experiment to another, in order to derive the related relaxation curves at each methine carbon site. NOE experiments were recorded in an interleaved manner: one scan with ^1H saturation during the SAT delay, and one scan without ^1H saturation. Quadrature detection in ω_1 was performed by incrementing the phase of the 90° ^{13}C pulse that precedes the t_1 evolution period. WALTZ-16 decoupling (Shaka et al., 1983) of carbon resonances was used during detection. The basic phase cyclings are summarized below. They were completed by a CYCLOPS scheme. In (a), the basic phase cycling is: φ1 = (x,–x); φ3 = (y,–y); φ4 = (y,y,–y,–y); φ5 = (x,x,x,x,–x,–x,–x,–x); φ6 = (–x,–x,x,x,x,x,–x,–x). In (b), the basic phase cycling is: φ1 = (x,–x); φ2 = f5 = (x,x,–x,–x); φ3 = (y,–y); φ4 = (y,y,y,y, –y,–y,–y,–y); φ6 = (x,x,x,x,–x,–x,–x,–x). In (c), the basic phase cycling is: φ1 = (y,–y); φ2 = (x,x,–x,–x); φ3 = (x,–x,–x,x).

chromophore which exhibits antitumour antibiotic properties. The apo-protein is essential for the stability and transport of its chromophore and has no cytotoxic activity (Kappen et al., 1980). Previous ^{1}H NMR (Adjadj et al., 1992a,b) and crystallographic (Teplyakov et al., 1993) studies of apo-neocarzinostatin suggest that the loops involved in the active site (Kim et al., 1993) are flexible and that this enhanced mobility may be related to the biological function of the protein. In order to investigate internal motions of apo-neocarzinostatin, nearly complete assignment of ^{13}C resonances was achieved (Lefèvre et al., 1994). In this paper, ^{13}C relaxation constants are interpreted in terms of the so-called model-free spectral density functions, using two or three adjustable parameters for the description of the internal motion (Lipari and Szabo, 1982; Clore et al., 1990a). Values of the order parameters S^2 (or S^2_{fast} and S^2_{slow}, hereafter abbreviated as S^2_f and S^2_s, respectively) and the effective internal correlation time τ_e (or τ_s) are obtained from a straightforward solution of the relaxation equations for R1 and NOE (or R1, R2 and NOE for the three-parameter case). In addition, the exchange contribution to R2, related to slow conformational changes, can be estimated when the two-parameter spectral density function is considered. Otherwise, this contribution should be assumed to be negligible. These data are discussed with reference to structural and dynamic information derived from X-ray and NMR studies.

Materials and Methods

Sample preparation

Holo-neocarzinostatin (NCS) was purchased from Kayaku Antibiotics Co. (Tokyo), and purified to homogeneity as described previously (Favaudon, 1983). Apo-NCS was prepared by acidic methanol extraction of the chromophore (Kappen et al., 1980) and subsequently purified following the same method as used for holo-NCS. Longitudinal relaxation measurements were performed on two samples of apo-NCS which were degassed and then sealed under argon. Protein concentrations were 9 and 7 mM in D_2O, at pH 5.5. For technical reasons, transverse relaxation and heteronuclear NOE measurements could be performed only on the second sample.

NMR spectroscopy

Heteronuclear ^{1}H-^{13}C experiments were carried out at 308 K on a Varian Unity500 spectrometer, equipped with a pulsed field gradient triple resonance probe. T1, T2 and NOE experiments were acquired with spectral widths of 5500 and 4000 Hz in the ^{1}H and ^{13}C dimensions, respectively. The ^{1}H carrier was placed on the residual HDO resonance (4.74 ppm at 308 K) and the ^{13}C carrier was set at 55 ppm. All spectra were acquired in the phase-sensitive mode by using hypercomplex quadrature detection in the ω_1 dimension. During acquisition, carbon resonances were decoupled with the WALTZ-16 scheme (Shaka et al., 1983).

The pulse sequences used to measure the relaxation parameters for the methine carbons of apo-neocarzinostatin are similar to those of Palmer et al. (1991) and are depicted in Fig. 1. They involve DEPT-type transfer of magnetisation and allow suppression of unwanted ^{1}H-^{12}C resonances prior to detection (Sklenář et al., 1987; Nirmala and Wagner, 1988,1989). This was realised by storing the carbon signals of interest along the z-axis and applying a 3 ms purge pulse, followed by a 0.5 ms z-gradient pulse of 0.2 T/m. Homogeneity was then recovered during a 3 ms delay. The solvent signal was also eliminated by this procedure. The $1/2J_{CH}$ periods in DEPT schemes were taken to be 3.3 ms. For methine ^{13}C, the contribution of chemical shift anisotropy (CSA) to the relaxation is expected to be small (Palmer et al., 1991), so experiments have not been modified to suppress cross-correlation effects between dipolar interactions and CSA (Kay et al., 1992; Palmer et al., 1992). Two spin-lock pulses with quadrature phases and a gradient pulse followed by a fixed recovery delay were inserted at the beginning of the sequence to establish the same initial ^{1}H state of magnetisation before each experiment.

Two spectra, one with and one without ^{1}H saturation, were recorded in an interleaved manner to yield heteronuclear steady-state ^{13}C-$\{^{1}H\}$ NOEs (Fig. 2). Full ^{1}H saturation was achieved by 90° pulses applied every 7 ms during 4 s (about seven times the mean methine carbon T1). The total acquisition time was approximately 81 h. Four independent experiments were recorded with the second sample, so as to reduce the experimental uncertainties on the heteronuclear NOE enhancements (Palmer et al., 1991).

During the recovery delay in T1 experiments, proton saturation was performed by means of 90° pulses, spaced 7 ms apart, in order to obtain monoexponential evolution of carbon magnetisation (Solomon, 1955; Kay et al., 1987). The recovery delay between scans was 2.5 s. Eleven experiments were recorded, with relaxation delays T of 0.01, 0.1, 0.2, 0.3, 0.4, 0.5, 0.7, 0.9, 1.1, 1.5 and 2 s (Fig. 3). The experiment with the smallest delay (0.01 s) was repeated twice when using the first sample. A second independent set of 11 measurements was done with the second sample. The relaxation delays were chosen randomly to compensate for possible systematic instrumental drift. The total data collection time was 15 days for each series.

T2 experiments were performed, on the second sample, with a CPMG spin-echo period ζ of 0.25 ms. Defocusing under heteronuclear coupling, which may affect the measured transverse rates (Peng et al., 1991), was negligible. Use of this spin-echo period also minimized the contribution of diffusion (Palmer et al., 1991). The period between scans was equal to 1.8 s. Nine experiments were

recorded, with relaxation delays T of 1, 5, 10, 15, 20, 30, 40, 50 and 60 ms (Fig. 3), resulting in a total data collection time of about eight days.

All spectra were recorded as 64 complex t_1 increments with 256 scans per increment and 4096 points in t_2. Data processing was carried out on a Sun Sparc2 workstation using the available Varian software (Vnmr 4.3). Squared cosine and cosine functions were applied on the FIDs in the t_2 and t_1 dimension, respectively. Baseline correction, using a third-order polynomial fitting, was performed prior to the second Fourier transformation.

Data analysis

All calculations were done on a PC (486-DX-II) using in-house programs written in the C programming language. Algorithms for random number generators used in the Monte Carlo simulations and fitting routines were taken from the Numerical Recipes (Press et al., 1986).

In T1 or T2 experiments, the detected signal is amplitude-modulated under longitudinal or transverse carbon relaxation, respectively, during a delay T which is parametrically varied from one spectrum to another. Signal intensities were fitted to the following equations:

$$I(T) = I_\infty + (I_0 - I_\infty)\exp(-R1 \times T) \quad (1)$$

for T1 experiments, and

$$I(T) = I_0 \exp(-R2 \times T) \quad (2)$$

for T2 experiments, where R1 and R2 are the longitudinal and transverse carbon relaxation rates, respectively (R1 = 1/T1; R2 = 1/T2). The initial value for the peak intensity is I_0, and the steady-state value is I_∞. Equation 2 assumes that the transverse magnetisation decays to a zero steady-state value. This assumption is not necessarily justified (Stone et al., 1992). In fact, the present data (Fig. 3) do not justify use of a three-parameter equation for transverse relaxation. In most cases, a three-parameter fit provided a steady-state value close to zero, within the standard deviation for this parameter. For long decaying magnetisation (such as for Ala[1]), however, apparently a significant non-zero steady-state value could be obtained. This is in fact due to the limited sampling of the relaxation decay used here. Thus, for consistency, we chose to fit all R2 data with a two-parameter equation. This is also justified by the Monte Carlo simulations performed on these data (vide infra).

^{13}C-{^1H} NOEs are calculated from:

$$\eta = \left(\frac{I_{sat}}{I_{unsat}} - 1\right) \quad (3)$$

where I_{sat} and I_{unsat} are intensities corresponding to spectra with and without ^1H saturation, respectively.

Since an individual resonance exhibits the same line shape in different T1, T2 or NOE spectra (Barbato et al., 1992; Constantine et al., 1993), intensities can be gauged by cross-peak heights (Palmer et al., 1991), integrals along F2 traces (Peng and Wagner, 1992b) or volumes (Clore et al., 1990b; Nicholson et al., 1992). However, the former appear to be more reliable, especially when resonances are not well separated as is often the case for proteins (Palmer et al., 1991; Barbato et al., 1992; Constantine et al., 1993). Errors in cross-peak maxima are estimated by measuring the root-mean-square (rms) baseline noise on each spectrum. Levenburg–Marquardt nonlinear least-squares fitting (Press et al., 1986) of peak heights according to Eqs. 1 and 2 yields carbon relaxation rates R1 and R2, respectively. Standard deviations in the optimised parameters obtained from the nonlinear fitting procedure are compared to those evaluated by Monte Carlo simulations as described by Palmer et al. (1991). Optimisation

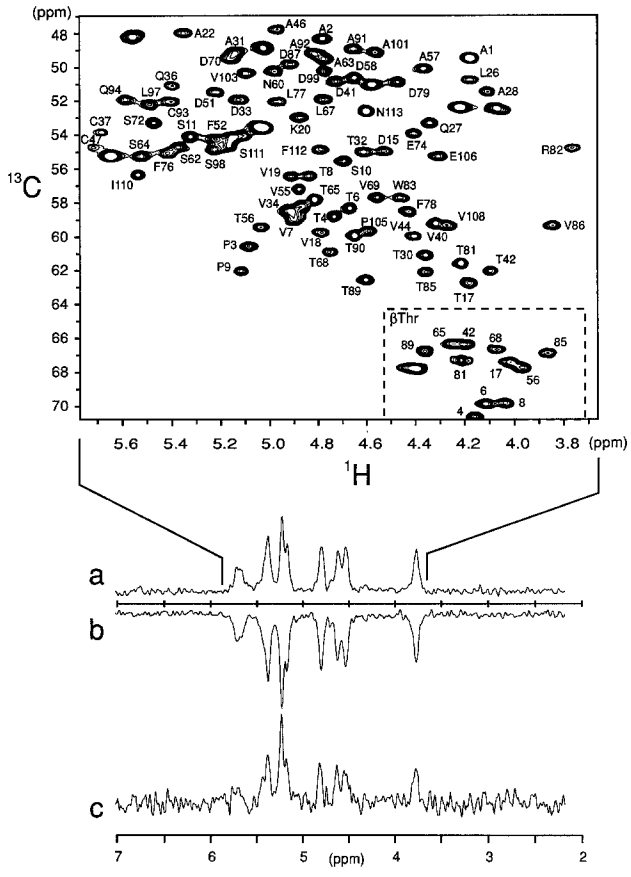

Fig. 2. Typical proton–carbon correlated spectrum with assignments. Upper part: typical reference spectrum of the heteronuclear NOE experiment, acquired and processed as described in the experimental section. Note that the two cross peaks corresponding to Arg^{71}-C^α and Pro^{49}-C^α lie outside the displayed region. Lower part: a typical trace of the NOE experiment through the cross peaks corresponding to Ser^{98}, Phe^{112} and Arg^{82}. The other peaks of the trace correspond to nearest cross-peak tails. (a) Trace of the reference spectrum; (b) trace of the steady-state NOE spectrum; (c) trace of the difference spectrum. Note that the latter trace is the sum of the four NOE experiments performed.

of the spectrum baseline correction significantly reduces the difference between these two error estimations. Systematic experimental errors in general increase the standard deviation of the fit. Also, incorrectness in the model describing the data may be enlightened by an abnormal large standard deviation obtained from the fitting algorithm. In particular, multiexponential decaying behaviour as well as nonzero steady-state transverse magnetisation may be discovered. The final standard deviations obtained from the least-square fitting procedure generally agree with the errors estimated by Monte Carlo simulations, using the models described in Eqs. 1 and 2 for R1 and R2, respectively. A more accurate modelling of our data is therefore not necessary. Uncertainties in the NOEs are estimated from a Monte Carlo simulation using 1000 intensities generated from a Gaussian distribution for each peak. The uncertainty in intensities is taken as the baseline noise standard deviation.

Methine carbon relaxation is mainly caused by the spatial reorientation of the internuclear C-H vector (connecting the carbon atom to its directly bound proton) (Wagner and Wüthrich, 1986; London, 1989; Palmer et al., 1991). The spectral density function J(ω) characterises the frequency spectrum of this motion. Relaxation rates R1 and R2 and heteronuclear steady-state NOEs are related to J(ω) values at five frequencies which correspond to transitions in the ^1H-^{13}C spin system (Abragam, 1961). Assuming that only dipolar and CSA interactions modulate the local magnetic field at each methine carbon site, the longitudinal (R1) and transverse (R2) relaxation rates, and the NOE are given by Eqs. 4–6:

$$R1 = \frac{D_{CH}^2}{4}\left\{J(\omega_H - \omega_C) + 3J(\omega_C) + 6J(\omega_H + \omega_C)\right\} + \Delta\delta^2\omega_C^2 J(\omega_C) \quad (4)$$

$$R2 = \frac{D_{CH}^2}{8}\left\{4J(0) + J(\omega_H - \omega_C) + 3J(\omega_C) + 6J(\omega_H) + 6J(\omega_H + \omega_C)\right\} + \frac{\Delta\delta^2\omega_C^2}{6}\left\{4J(0) + 3J(\omega_C)\right\} \quad (5)$$

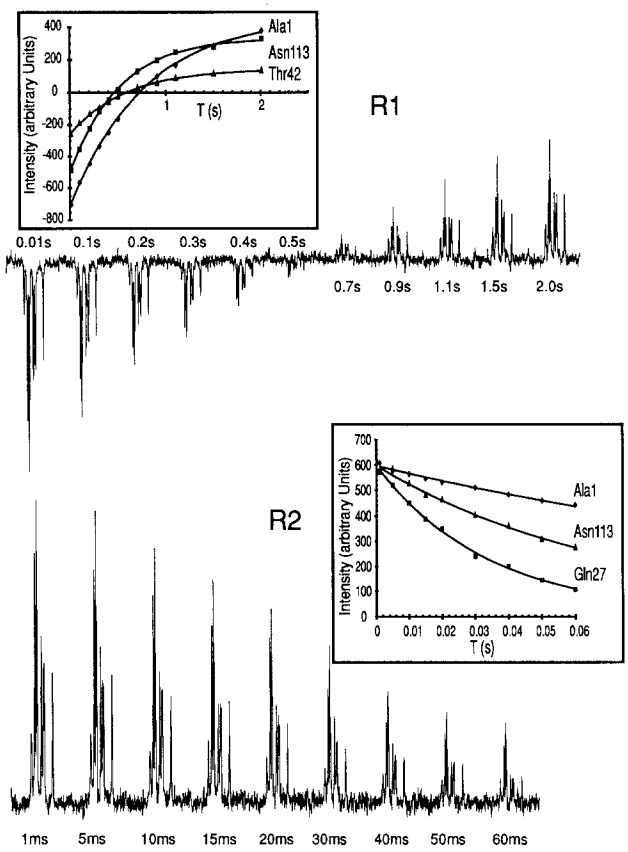

Fig. 3. Typical traces and decay curves of R1 and R2 experiments. The selected trace is the same as in Fig. 2. The relaxation delays are indicated, for each experiment, below each trace. The decay curves correspond to the lowest, highest and an intermediate value for R1 and R2. Note that the experimental intensities have been normalised for R2.

$$\eta = \frac{\gamma_H}{\gamma_C}\frac{6J(\omega_H + \omega_C) - J(\omega_H - \omega_C)}{J(\omega_H - \omega_C) + \left[3 + 4\Delta\delta^2\omega_C^2 D_{CH}^{-2}\right]J(\omega_C) + 6J(\omega_H + \omega_C)} \quad (6)$$

Note that R1 and η are related by:

$$R1 \times \eta = \frac{\gamma_H}{\gamma_C}\frac{D_{CH}^2}{4}\left\{6J(\omega_H + \omega_C) - J(\omega_H - \omega_C)\right\} \quad (7)$$

γ_H and γ_C are the gyromagnetic ratios of ^1H and ^{13}C (2.6752×10^8 $s^{-1}T^{-1}$ and 6.728×10^7 $s^{-1}T^{-1}$, respectively), ω_H and ω_C are the nuclear ^1H and ^{13}C Larmor pulsations ($\omega_H = 2\pi\times499.843$ MHz, $\omega_C = 2\pi\times125.892$ MHz), D_{CH} = 1.46×10^5 s^{-1} for a ^1H-^{13}C system with a carbon–hydrogen bond length of 0.109 nm, and $\Delta\delta$ = 25 ppm for methine α-carbon nuclei.

In addition to the contributions described above, the transverse relaxation rate R2 may contain a contribution of slow conformational exchange $R2_{ex}$, corresponding to motions on a time scale of 10^{-6} to 10^{-3} s.

Mapping of the spectral density function (Peng and Wagner, 1992a) requires other relaxation parameters than T1, T2 and ^{13}C-{^1H} NOE to be measured, but has the advantage that it does not make a hypothesis on the form of J(ω). However, this approach could not be followed here due to the long measurement times associated with experiments at natural ^{13}C abundance. Thus, the spectral density function had to be expressed with reference to a statistical motional model involving a limited number of parameters. The 'model-free' formalism of Lipari and

Szabo (1982) used here makes the assumption that overall and internal motions contribute independently to the reorientational time correlation function of C-H vectors and that internal motions occur on a much faster time scale than the global rotation of the molecule. For an isotropically tumbling protein, one obtains:

$$J(\omega) = \frac{2}{5}\left\{S^2 \frac{\tau_c}{1+(\omega\tau_c)^2} + (1-S^2)\frac{\tau}{1+(\omega\tau)^2}\right\} \quad (8)$$

with $\tau^{-1} = \tau_c^{-1} + \tau_e^{-1}$. The order parameter S^2 describes the relative amplitude of internal motions and ranges from 0 to 1. The effective correlation time τ_e has less immediate physical meaning, since it is related both to amplitude and rate of the internal dynamics. Thus, interpretation of τ_e values can only be done within a specific motional model.

For some of the residues, the simple form of Eq. 8 turns out to be insufficient to agree with the whole set of experimental data. This occurs when residues exhibit internal motions in a time window close to 1 ns. In that case, the correlation function becomes biexponential and the simplest expression for the spectral density function consistent with the available relaxation data is (Clore et al., 1990a):

$$J(\omega) = \frac{2}{5}\left\{S_f^2 S_s^2 \frac{\tau_c}{1+(\omega\tau_c)^2} + S_f^2(1-S_s^2)\frac{\tau}{1+(\omega\tau)^2}\right\} \quad (9)$$

with $\tau^{-1} = \tau_c^{-1} + \tau_s^{-1}$, where S_f^2 and S_s^2 are the generalised order parameters for fast (picosecond time scale) and slow (τ_s, nanosecond time scale) internal motion, respectively. Equation 9 assumes that the fast motion components drive ^{13}C relaxation to the extreme narrowing limit.

Results and Discussion

Relaxation parameters

Apo-neocarzinostatin is composed of 113 amino acid residues, 15 of which are glycines. Relaxation of the remaining 98 methine C^α could theoretically be analysed. In practice, however, nine cross peaks correspond to contributions from two residues, so that the derived relaxation parameters reflect an uncertain combination of the dynamical properties of these residues (Van Mierlo et al., 1993). Cys^{88} C^α could still not be identified, but Arg^{71} and Pro^{49} C^α, which lack in the previous assignment (Lefèvre et al., 1994), have been tentatively assigned to the cross peaks at (ω_1 = 56.35 ppm, ω_2 = 2.26 ppm) and (ω_1 = 61.35 ppm, ω_2 = 2.30 ppm), respectively. Finally, a total of 79 ^1H-^{13}C resonances were sufficiently intense and well resolved to yield reliable values for all relaxation parameters with errors less than 4% in the R1 and R2 rates, and between 10–15% in the NOEs.

Figure 4 displays R1, R2 and NOE parameters as a function of the amino acid sequence. There is not much variation in R1 rates. R2 and NOE parameters exhibit larger changes, especially between N- or C-terminal residues and the rest of the protein. As expected, extremities of the polypeptide chain exhibit clearly increased mobility. The main changes concern Ala^1–Pro^3 of the N-terminal region, but only Asn^{113} of the C-terminus. Deeper insight into the internal motions of apo-neocarzinostatin requires calculation of the model-free parameters and estimation of the contribution from chemical exchange $R2_{ex}$.

Estimation of the overall rotational correlation time τ_c

Interpretation of relaxation data in terms of Lipari–Szabo parameters first requires an estimation of the global reorientational correlation time of the protein, τ_c. A standard approach consists of using R2/R1 ratios corresponding to residues in well-defined secondary structures, or more generally to residues for which relaxation is expected to be predominantly driven by restrained fast internal motions, while exchange processes are negligible (Kay et al., 1989; Clore et al., 1990b; Palmer et al., 1991). This strategy leads to rotational correlation times that seem overestimated as compared to either fluorescence results (Palmer et al., 1993; Kemple et al., 1994) or Stokes–Einstein model values (Berglund et al., 1992; Stone et al., 1993). For apo-neocarzinostatin, the Stokes–Einstein method (Cantor and Schimmel, 1980) yields a τ_c equal to 3.7 ns, while relaxation data yield a τ_c equal to

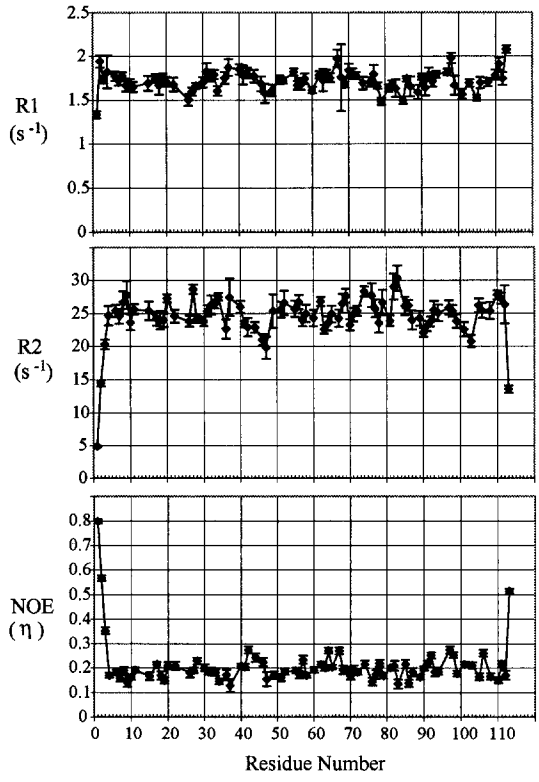

Fig. 4. Relaxation parameters R1, R2 and NOE for the methine carbons of apo-neocarzinostatin, versus the amino acid sequence.

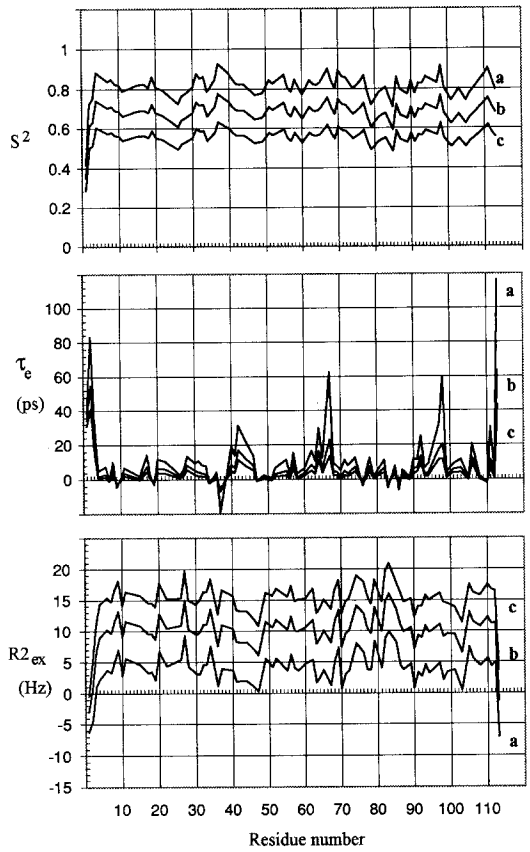

Fig. 5. Model-free parameters (S^2 and τ_e) and exchange contribution to the transverse relaxation rate ($R2_{ex}$) for the methine C^α of apo-neocarzinostatin, versus the amino acid sequence. The two-parameter spectral density function described in Eq. 8 has been used. Results are shown for three different values assumed for the overall tumbling time τ_c ((a) τ_c = 5.7 ns; (b) τ_c = 4.5 ns; (c) τ_c = 3.5 ns). Note that the peak values of τ_e for residues 67 and 98 are not significant. They are associated with large errors.

5.7 ns. It has been suggested that the differences in τ_c values observed between NMR and other methods may be related to the high concentrations used for NMR spectroscopy (Cheng et al., 1993; Constantine et al., 1993). This effect may be due to an increase in viscosity and/or to some hydration effects (Kemple et al., 1994).

In fact, Fig. 5 shows that a varying τ_c leads to similar relative variations of S^2, τ_e or $R2_{ex}$ parameters along the polypeptide chain (Powers et al., 1992; Van Mierlo et al., 1993; Jones et al., 1994). Conversely, the absolute values of the order parameter S^2 are much affected by changes in the τ_c value. Thus, in the case where τ_c is equal to 5.5 ns, most of the residues indeed have $S^2 \geq 0.75$, consistent with previous results reported for several other proteins (Wagner, 1993). If τ_c = 3.5 ns, the corresponding order parameters range from 0.50 to 0.65. But within the 'wobbling-in-a-cone' model (Lipari and Szabo, 1982), the semi-angles are abnormally large (about 45°). Therefore, the value for τ_c obtained from the R2/R1 ratios, 5.7 ns, seems more appropriate. This value will be used in the following.

Determination of the microdynamical parameters

Calculations of the model-independent parameters followed a slightly different approach from that usually described. In a first step, the correlation function for the internal motions was assumed to be described by a single exponential, i.e., the two-parameter spectral density function given in Eq. 8 is valid. The corresponding model-free parameters S^2 and τ_e were determined from the NOE (η) and R1 data alone. Then, R2 was calculated from Eq. 5 and compared with the experimental value for each residue. In general, the calculated R2 rate is smaller than the measured transverse rate. The difference is interpreted as the exchange contribution $R2_{ex}$. Sometimes, however, the calculated rate R2 is larger than the experimental one. In those cases, the simple two-parameter density function, Eq. 8, clearly does not hold and Eq. 9 must be used. Estimation of the three unknown parameters (S_f^2, S_s^2 and τ_s) simultaneously requires the three experimental data R1, R2 and NOE (η). $R2_{ex}$ must therefore be assumed to be zero.

Figure 6 shows the (η, R1) experimental data points for the methine C^α, plotted together with constant S^2 and τ_e lines calculated for τ_c = 5.7 ns. These data are consistent with restrained fast motion; S^2 is around 0.85 and τ_e is smaller than 20 ps for most of the C^α. Note furthermore that, within experimental errors, all data lie in allowed regions defined by $S^2 \leq 1$ and $\tau_e \geq 0$, supporting the choice for the τ_c value.

It is noteworthy that calculation of the S^2 and τ_e parameters is done in the ($R1 \times \eta$, R1) plane (Dellwo and Wand, 1989; Kemple et al., 1994) rather than in the (η, R1) plane displayed in Fig. 6. In the former plane, the constant τ_e lines are indeed straight lines, with slopes

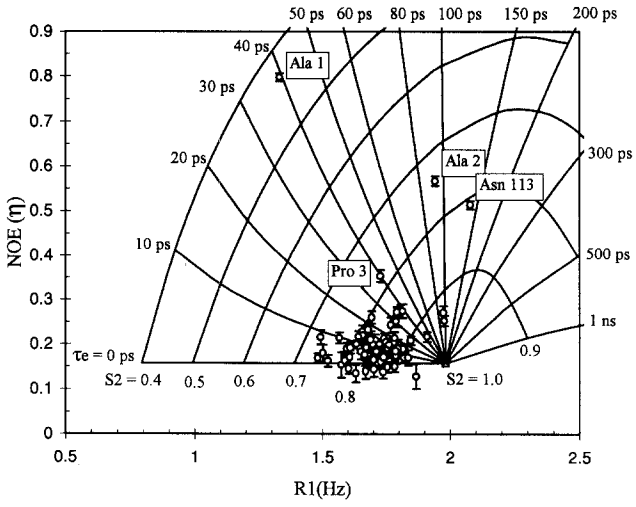

Fig. 6. Representation of the experimental data in the (R1, NOE) plane. Theoretical curves are drawn for different values of τ_e (from 0 to 1 ns) and S^2 (from 0.4 to 1). They are calculated using the two-parameter spectral density function, Eq. 8. Note that for S^2 = 1, all curves reduce to a single point.

TABLE 1
MODEL-FREE ORDER PARAMETERS AND CORRELATION TIMES FOR C^{α}

	S^2	$\sigma(S^2)$	τ_e (ps)	$\sigma(\tau_e)$	$R2_{ex}$ (Hz)	$\sigma(R2_{ex})$		S^2	$\sigma(S^2)$	τ_e (ps)	$\sigma(\tau_e)$	$R2_{ex}$ (Hz)	$\sigma(R2_{ex})$
Ala[1]	0.432	0.014	39.5	2.4	−6.9	0.4	Ser[62]	0.871	0.021	20.3	5.8	3.9	0.9
Ala[2]	0.743	0.023	92.4	17.7	−5.5	0.8	Ala[63]	0.849	0.061	12.6	51.3	0.3	1.8
Pro[3]	0.776	0.018	40.0	4.6	−0.2	0.8	Ser[64]	0.846	0.025	35.0	7.9	1.2	1.3
Thr[4]	0.912	0.100	6.7	169.3	0.8	3.0	Thr[65]	0.860	0.027	15.0	4.3	2.3	1.4
Thr[6]	0.881	0.029	9.3	6.7	2.3	1.2	Leu[67]	0.929	0.034	94.2	117.8	−0.2	1.6
Val[7]	0.866	0.027	0.2	4.9	1.9	1.4	Thr[68]	0.868	0.175	11.8	194.7	3.7	4.8
Thr[8]	0.878	0.023	12.4	5.3	3.7	1.9	Val[69]	0.827	0.016	8.8	2.8	5.9	1.1
Pro[9]	0.850	0.038	−5.1	6.0	5.5	2.4	Arg[70]	0.920	0.037	7.2	64.7	−0.9	1.3
Ser[10]	0.847	0.027	1.3	3.2	1.4	1.3	Arg[71]	0.889	0.031	14.0	9.8	1.5	1.4
Ser[11]	0.816	0.028	7.7	2.8	4.2	1.1	Ser[72]	0.884	0.019	10.0	4.4	2.2	0.9
Asp[15]	0.848	0.042	2.4	5.3	3.2	1.8	Glu[74]	0.826	0.037	14.3	6.0	6.6	1.3
Thr[17]	0.851	0.026	16.8	4.6	1.8	1.3	Phe[76]	0.864	0.029	−4.3	6.3	5.1	2.0
Val[18]	0.835	0.052	3.0	18.8	2.1	2.0	Leu[77]	0.894	0.053	7.0	69.8	2.3	2.0
Val[19]	0.890	0.023	−3.6	6.0	0.7	1.2	Phe[78]	0.807	0.019	13.9	3.0	2.3	1.5
Lys[20]	0.836	0.027	13.8	4.4	5.3	0.9	Asp[79]	0.743	0.021	1.7	1.6	7.1	2.1
Ala[22]	0.821	0.040	12.2	5.4	3.0	1.5	Thr[81]	0.804	0.020	9.2	2.2	2.7	0.9
Leu[26]	0.748	0.035	3.5	3.0	4.2	1.3	Arg[82]	0.822	0.022	12.6	4.5	7.4	1.9
Gln[27]	0.790	0.027	6.4	2.4	7.9	1.0	Trp[83]	0.832	0.054	−5.6	56.4	8.5	2.3
Ala[28]	0.803	0.018	15.3	3.0	3.0	0.8	Thr[85]	0.728	0.022	8.2	2.3	6.9	1.5
Thr[30]	0.836	0.030	11.3	4.3	1.8	1.0	Val[86]	0.886	0.018	−7.6	34.6	3.0	0.9
Ala[31]	0.905	0.043	14.2	77.9	1.6	1.4	Asp[87]	0.821	0.056	6.2	5.0	2.4	2.0
Tyr[32]	0.883	0.032	10.6	7.8	3.1	1.7	Thr[89]	0.798	0.039	1.3	2.4	3.3	1.6
Asp[33]	0.890	0.027	9.9	6.2	3.1	0.9	Thr[90]	0.867	0.017	14.3	3.6	−0.7	0.8
Val[34]	0.813	0.027	−2.5	2.8	6.2	0.9	Ala[91]	0.801	0.043	12.6	4.8	2.0	1.4
Gln[36]	0.875	0.033	5.1	8.6	−0.3	1.8	Ala[92]	0.855	0.036	30.2	17.9	1.2	1.3
Cys[37]	0.957	0.064	−32.6	228.5	2.4	3.3	Cys[93]	0.851	0.032	7.8	5.7	3.1	1.6
Val[40]	0.905	0.030	25.8	20.6	2.2	1.2	Gln[94]	0.888	0.021	11.2	5.8	1.8	1.3
Asp[41]	0.874	0.049	17.1	43.0	0.4	1.4	Leu[97]	0.855	0.019	38.7	6.9	3.3	1.2
Thr[42]	0.851	0.031	37.2	12.2	0.5	1.6	Ser[98]	0.940	0.021	96.1	86.0	0.6	1.1
Val[44]	0.849	0.037	26.2	10.2	0.5	1.3	Asp[99]	0.831	0.052	4.9	4.4	2.0	1.7
Ala[46]	0.817	0.043	15.9	6.8	−0.5	1.4	Ala[101]	0.765	0.029	9.7	2.6	2.5	1.3
Cys[47]	0.795	0.056	−0.7	6.6	−1.0	2.2	Asn[103]	0.827	0.021	13.3	3.6	−1.0	1.1
Pro[49]	0.805	0.034	3.0	3.1	4.2	2.6	Pro[105]	0.765	0.019	0.9	2.3	6.1	1.2
Asp[51]	0.871	0.025	1.1	5.8	2.7	1.4	Glu[106]	0.805	0.032	23.1	5.6	4.2	1.4
Phe[52]	0.854	0.017	8.2	3.6	4.1	1.9	Val[108]	0.854	0.023	2.4	3.8	3.0	1.4
Val[55]	0.900	0.021	15.0	6.0	2.1	1.3	Ile[110]	0.903	0.029	−3.2	57.3	4.1	1.1
Thr[56]	0.834	0.026	3.9	4.2	4.8	1.3	Ser[111]	0.931	0.030	43.9	96.6	2.8	1.1
Ala[57]	0.811	0.031	17.4	5.2	2.7	1.3	Phe[112]	0.871	0.037	4.7	9.4	3.5	3.3
Asp[58]	0.872	0.029	4.3	4.2	2.1	1.5	Asn[113]	0.812	0.010	137.6	19.0	−8.2	0.6
Asn[60]	0.796	0.019	7.0	2.6	3.4	1.4							

The listed parameters were obtained using the two-parameter spectral density function of Eq. 8. Calculations were performed using $\tau_c = 5.7$ ns. The exchange contribution to the transverse relaxation rate, $R2_{ex}$, is the difference between the value calculated from Eq. 5 and the experimental one. Note that when this contribution is negative within experimental error, the corresponding relaxation data have been reinterpreted using the three-parameter spectral density function, Eq. 9. The uncertainty for parameter X is $\pm\sigma(X)$. σ is estimated as described in the text.

independent of S^2, which in addition all intersect at the unique point corresponding to $S^2 = 1$. The slope of each line is given by:

$$s = \frac{R1 \times \eta - R1_0 \times \eta_0}{R1 - R1_0} \qquad (10)$$

where R1 and η are the experimental values and $R1_0$ and η_0 are the longitudinal relaxation rate and NOE, respectively, calculated for $S^2 = 1$. From Eqs. 4, 7 and 8, s may be expressed as a nonlinear function solely dependent on τ_e. This parameter is thus obtained, with any desired accuracy, by successive approximations. Finally, S^2 is analytically derived from Eq. 7, which is linear for this parameter. During this procedure, τ_e is allowed to be slightly negative and S^2 slightly greater than 1. This allows experimental errors to be accounted for.

When the spectral density function has to be expressed as Eq. 9, exact solutions for S_f^2, S_s^2 and τ_s can be found noticing that Eq. 9 is identical to Eq. 8, provided S_s^2 and τ_s are substituted for S^2 and τ_e, respectively, and that S_f^2 is factored. Thus, the same procedure as described above is used to compute S_s^2 and τ_s with $R1 \times \eta$ and R1 as input data, but each divided by an initial guessed value for S_f^2. Then a transverse relaxation rate, $R2_{cal}$, is computed from Eq. 5 and compared to the experimental value, $R2_{exp}$. The

procedure is repeated with another guessed value for S_f^2 until $|R2_{cal} - R2_{exp}|$ is smaller than a given tolerance.

Finally, the uncertainties for the parameters are obtained by a Monte Carlo simulation. For this simulation, 500 Gaussian random distributions of the relaxation data are generated for each residue. Standard deviations of the Gaussian distributions are the error estimates for the relaxation rates and NOEs.

Internal dynamics on the ps to ns time scale

The microdynamical parameters obtained using the two-parameter spectral density, Eq. 8, are given in Tables 1 and 2 for the methine carbons of the backbone and for the 11 threonine side-chain C^β, respectively. A graphical display of these parameters versus the amino acid sequence is given in Fig. 5.

Three residues of the polypeptide chain extremities (Ala^1, Ala^2 and Asn^{113}) and eight of the 11 threonine C^β exhibit a significant negative exchange contribution $R2_{ex}$. This indicates that these residues are subjected to an internal motion containing both fast and slow components (Clore et al., 1990a). For these residues, the spectral density function given by Eq. 9 has been used. The corresponding parameters are given in Table 3.

For the backbone of the protein, excluding the few terminal residues, no immediate correlation between the model-free parameters and the secondary structure of apo-neocarzinostatin can be extracted from Fig. 5, due to the weak scattering of these parameters. However, the figure points out slight trends concerning the loops that are involved in the active site. The β-ribbon that runs from residue 37 to 47 (Fig. 7) appears constrained (high order parameters), but it displays τ_e values significantly larger than average for residues 42–44. Except in the hairpin region (residues 41–43), this loop has previously been reported to be quite rigid on the basis of carbon secondary chemical shifts (Lefèvre et al., 1994) and rms deviations derived from the NMR three-dimensional structures (Adjadj et al., 1990,1992a). A slight but significant decrease in the order parameters for the loops comprising residues 72–87 and 97–107 (Fig. 7) also indicates an enhanced flexibility, in agreement with other NMR (Adjadj et al., 1992a,b; Lefèvre et al., 1994) and crystallographic (Teplyakov et al., 1993) studies. The related internal correlation times are small, except for residues 97 and 98 which display τ_e values above the average. Internal mobility of these two regions may play a role in chromophore binding, and furthermore, is likely to enable structural rearrangements in the holo state (Takashima et al., 1991; Adjadj et al., 1992a).

The terminal residues exhibit dynamics that was already predicted from a crude examination of the corresponding C^α relaxation data. N-terminal residues display a smooth increase in the motional constraints over four residues; the S^2 values, taken as $S_f^2 \times S_s^2$ (Clore et al., 1990a), are 0.14 for Ala^1, 0.52 for Ala^2, 0.78 for Pro^3 and 0.91 for Thr^4. The C-terminal extremity is also relatively flexible ($S^2 = 0.47$), but is suddenly restrained at residue Phe^{112} ($S^2 = 0.87$). This may be due to the large number of hydrogen bonds, involving at least residues 108, 110 and 111, that stabilise the conformation of this terminal β-strand (Adjadj et al., 1992a).

The dynamic properties of most (8 of 11) side-chain C^β are clearly more complex than those of the majority of the backbone C^α, but resemble those of the few unconstrained C^α of Ala^1, Ala^2 and Asn^{113}. Both types of carbon display a slow motional component in the range between about 500 to 3000 ps. Noteworthy, the three terminal-residue C^α atoms display a τ_s close to 500 ps, while the values of τ_s for the C^β are more scattered. It should be mentioned at this point that the estimated model-free parameters depend on the assumption that the exchange contribution to the transverse relaxation rate, $R2_{ex}$, is negligible. If this is not true, the contribution of slow motions to the relaxation may be underestimated. Nevertheless, the S^2 parameter for all the threonine side-chain C^β is smaller than the average value for the backbone C^α, consistent with relatively unconstrained motion at these sites. In fact, large-amplitude motions (small S^2) seem to be correlated with complex local disorder. More specifically, the carbon nuclei present in constrained regions are expected to undergo unavoidable fast (picosecond time

TABLE 2
MODEL-FREE ORDER PARAMETERS AND CORRELATION TIMES FOR THE 11 THREONINE C^β

	S^2	$\sigma(S^2)$	τ_e (ps)	$\sigma(\tau_e)$	$R2_{ex}$ (Hz)	$\sigma(R2_{ex})$		S^2	$\sigma(S^2)$	τ_e (ps)	$\sigma(\tau_e)$	$R2_{ex}$ (Hz)	$\sigma(R2_{ex})$
Thr^4	0.780	0.023	1052	105	−7.3	0.5	Thr^{65}	0.814	0.025	40	8	1.8	0.9
Thr^6	0.821	0.034	1464	294	−6.4	0.7	Thr^{68}	0.756	0.046	12	4	3.6	1.5
Thr^8	0.792	0.168	2015	719	−6.7	3.8	Thr^{81}	0.775	0.045	9	3	2.7	1.3
Thr^{17}	0.856	0.020	350	75	−5.6	0.8	Thr^{85}	0.892	0.028	85	49	−3.2	1.0
Thr^{42}	0.879	0.029	95	55	−6.3	1.1	Thr^{89}	0.908	0.048	1254	474	−6.0	1.3
Thr^{56}	0.964	0.020	214	200	−6.1	0.9							

The listed parameters were obtained using the two-parameter spectral density function of Eq. 8. Calculations were performed using $\tau_c = 5.7$ ns. The exchange contribution to the transverse relaxation rate, $R2_{ex}$, is the difference between the value calculated from Eq. 5 and the experimental one. Note that when this contribution is negative within experimental error, the corresponding relaxation data have been reinterpreted using the three-parameter spectral density function, Eq. 9. The uncertainty for parameter X is $\pm\sigma(X)$. σ is estimated as described in the text.

TABLE 3
MODEL-FREE ORDER PARAMETERS AND CORRELATION TIMES FOR SLOW AND FAST MOTIONS OF CARBON NUCLEI

	S^2_{slow}	$\sigma(S^2_s)$	τ_{slow} (ps)	$\sigma(\tau_s)$	S^2_{fast}	$\sigma(S^2_f)$
Ala^1 C^α	0.364	0.016	418	8	0.385	0.009
Ala^2 C^α	0.704	0.022	390	28	0.734	0.017
Asn^{113} C^α	0.647	0.020	515	21	0.719	0.017
Thr^4 C^β	0.570	0.020	1413	133	0.801	0.014
Thr^6 C^β	0.630	0.025	2023	304	0.832	0.012
Thr^8 C^β	0.542	0.045	2842	317	0.828	0.023
Thr^{17} C^β	0.736	0.027	595	47	0.844	0.025
Thr^{42} C^β	0.790	0.030	628	70	0.766	0.027
Thr^{56} C^β	0.851	0.028	1007	173	0.828	0.026
Thr^{85} C^β	0.883	0.020	473	97	0.859	0.023
Thr^{89} C^β	0.754	0.044	2064	319	0.844	0.030

The listed parameters were obtained using the three-parameter spectral density function of Eq. 9. Slow motions are on the nanosecond time scale; fast motions are on the picosecond time scale. Calculations were done using $\tau_c = 5.7$ ns. The uncertainty for parameter X is $\pm\sigma(X)$. σ is estimated as described in the text.

scale) small-scale motions (S^2 in the range 0.80–0.95). In less rigid regions the internal motions become more complex, including slower components on the nanosecond time scale. In this latter case, the S^2 ($S_f^2 \times S_s^2$) values decrease only slightly to the range 0.6–0.8, except for extremely unconstrained residues such as the N-terminal Ala^1 in apo-NCS.

The model-free parameters related to the picosecond to nanosecond time scale (S^2 and τ_e), determined as described above, depend on the choice of a particular τ_c value, whereas the product $(1 - S^2) \times \tau_e$ does not (Fig. 8). Thus, on condition that $\tau_e \ll \tau_c$ and $\tau_e \times (\omega_H + \omega_C) \ll 1$ (extreme narrowing limit), $(1 - S^2) \times \tau_e$ provides a genuine reflection of local fast internal motions. In addition, Fig. 8 reveals a remarkably close correlation between the $(1 - S^2) \times \tau_e$ and NOE data along the protein sequence. It should be noted at this point that the motional parameters for eight threonine C^β do not follow this trend, in contrast to those of the three terminal-residue (Ala^1, Ala^2 and Asn^{113}) backbone C^α. However, as shown in Table 3, the C^β appear to have generally less mobility than the C^α. This suggests that heteronuclear steady-state NOEs could be used, with some caution, to derive qualitative information on the internal motions faster than the overall tumbling, ideally in the extreme narrowing limit. This could be generally true for backbone C^α atoms of the protein core.

Internal dynamics on the μs to ms time scale

Transverse relaxation is sensitive to motions on the microsecond to millisecond time scale if these produce changes in the resonance frequency. However, accurate information on the rates of the so-called 'exchange processes' cannot be derived without knowledge of the chemical shift differences between nuclear environments (Clore et al., 1990b; Palmer et al., 1991; Powers et al., 1992; Constantine et al., 1993). Furthermore, since $R2_{ex}$ terms are determined as the differences between experimental and calculated R2 rates during the optimisation procedure, they should be cautiously analysed (Cheng et al., 1993). Correct quantification of exchange phenomena implies performing other experiments, such as measuring the rotating frame relaxation times as a function of the spin-lock power (Deverell et al., 1970; Blackledge et al., 1993; Szyperski et al., 1993). Some information may also be obtained by performing a set of T2 experiments with different rates in CPMG pulse trains (Orekhov et al., 1994). However, $R2_{ex}$ values reflect motions slower than the overall tumbling, some of which may be implicated in the biological function of the protein. It is thus interesting to derive as much qualitative information as possible from $R2_{ex}$ parameters.

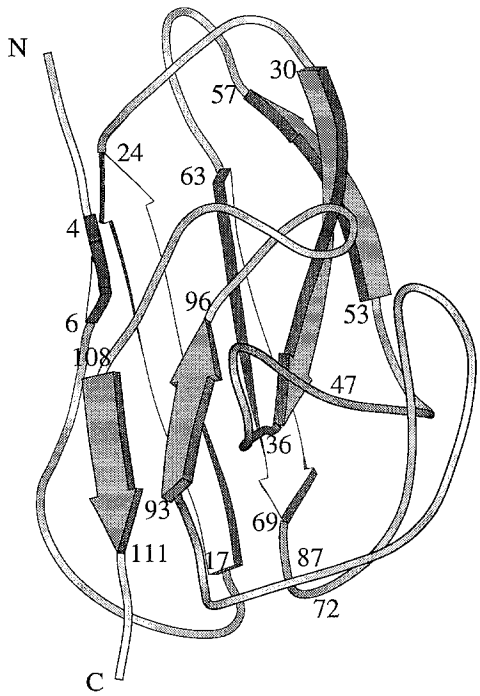

Fig. 7. Ribbon representation of the apo-neocarzinostatin solution structure, obtained by NMR (Adjadj et al., 1992a), pictured using the program MOLSCRIPT (Kraulis, 1991).

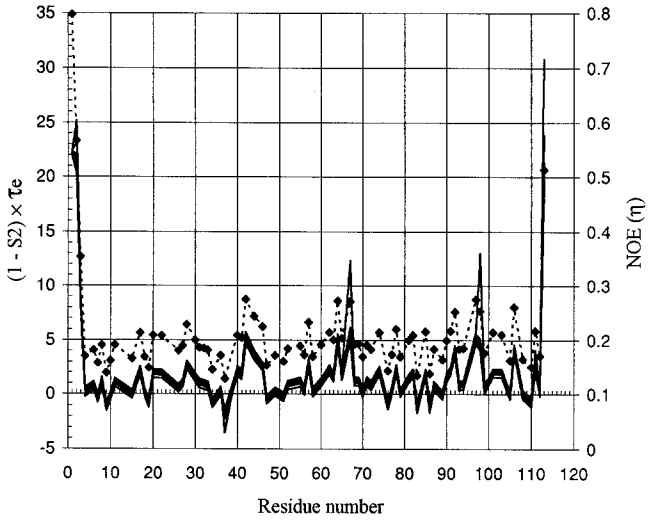

Fig. 8. Representation of the product $(1 - S^2)\times\tau_e$ obtained with different τ_e values. The product is compared with the experimental ^{13}C-{^1H} NOE. The estimated product values are shown versus the amino acid sequence of apo-neocarzinostatin (solid line) and compared to the experimental ^{13}C-{^1H} NOE (dotted line). The estimations for $(1 - S^2)\times\tau_e$ have been obtained from the experimental data, assuming seven different τ_e values ranging from 3 to 6 ns. The figure displays the remarkable independence of $(1 - S^2)\times\tau_e$ with respect to τ_e. The calculation tends to diverge for τ_e values larger than 6 ns for residues 67 and 98, but the associated errors (not shown) are large for these residues.

Previous studies have shown that exchange contributions may arise for residues in the vicinity of the binding site (Palmer et al., 1991,1993; Stone et al., 1993; Fushman et al., 1994), for loops involved in conformational equilibria (Kay et al., 1989; Clore et al., 1990b; Farrow et al., 1994), for structured regions which display breathing motions (Redfield et al., 1992; Cheng et al., 1993; Grasberger et al., 1993; Orekhov et al., 1994) or even for rigid sites in the vicinity of reorienting aromatic side chains (Constantine et al., 1993; Grasberger et al., 1993; Farrow et al., 1994). For backbone nuclei, these contributions have been reported to occur quite infrequently and to be weak compared to the related transverse relaxation rates.

For apo-NCS the largest contribution is around 8 Hz, as compared to a mean transverse relaxation rate of 26 Hz. Nine residues display a contribution larger than 6 Hz. Particularly, residues 69, 74, 79, 82, 83 and 85, belonging to one of the active loops (Adjadj et al., 1992a,b; Kim et al., 1993) exhibit the largest exchange contributions. Residues 105 and, to a lesser extent, 106 of the third loop (96 to 108) display also significant exchange contributions. In contrast, the first β-ribbon (residues 37 to 47) appears to be restricted on the microsecond to millisecond time scale.

Two additional residues (27 and 34) display an $R2_{ex}$ contribution larger than 6 Hz. They are located either in well-defined secondary structure or in an unstructured loop, but proximal aromatic ring reorientation of Tyr^{32} and Phe^{52} may contribute to the $R2_{ex}$ for Gln^{27} and Val^{34}, respectively.

Conclusions

The present work provides additional data pertaining to the relaxation properties of ^{13}C in a protein of about 10 kDa, in attempting to sample its internal motion. Because of the absence of isotopic enrichment, the experimental data remain limited to the measurement of longitudinal and transverse relaxation rates and ^{13}C-{^1H} NOEs. Nevertheless, in agreement with many other reports, using the model-free approach of Lipari and Szabo (1982), the internal motions in the picosecond to nanosecond range can be quantitatively analysed.

The backbone of NCS, a well-structured protein, is restrained to a large extent, with only small deviations in the amplitude $(1 - S^2)$ and characteristic internal correlation time (τ_e) along the polypeptide chain. However, despite the difficulties in correlating each parameter separately with the regular secondary-structure regions of the protein, differences could be pointed out between these structures and the loops involved in the binding site, the dynamical properties of which may be altered by the chromophore binding. The present work provides the basis for such an analysis.

Compared to the main structure, the terminal residues of the protein exhibit a quite different mobility. Their motions are composed of both fast and slow components, in the picosecond and 500 ps range, respectively. Most of the C^β side chains show quite similar motions, but the corresponding C^β-H bonds are clearly less restricted than the C^α-H bonds. These dynamical properties can be described as follows. C-H bonds within very constrained regions, such as the C^α-H, invariably display a restricted fast motion on the picosecond time scale. As constraints become relaxed, a slower motion on the nanosecond time scale, of still small amplitude, progressively contributes to the local mobility. ^{13}C NMR relaxation adequately samples both kinds of motions. However, the interpretation of the two S^2,τ parameters in physical space is not directly feasible. Conversely, molecular dynamics simulations are able to predict nuclear relaxation properties which then may be compared with experimental data. The present work provides the basis for such a comparison, dealing with a 10 kDa protein of well-known structure (Adjadj et al., 1992a; Teplyakov et al., 1993).

Acknowledgements

Financial support from the Ligue Nationale Francaise Contre le Cancer, the Institut Curie and INSERM allowed completion of this work.

Note added in proof

Recent time-resolved fluorescence measurements performed on a solution of apo-NCS at 300 K yielded a

rotational correlation time of $\tau_c = 5.8 \pm 0.2$ ns (P. Garcia, unpublished results), in close agreement with the value estimated from NMR data ($\tau_c = 5.7 \pm 0.12$ ns).

References

Abragam, A. (1961) *Les Principes du Magnétisme Nucléaire*, Presses Universitaires de France, Paris.

Adjadj, É., Mispelter, J., Quiniou, É., Dimicoli, J.L., Favaudon, V. and Lhoste, J.M. (1990) *Eur. J. Biochem.*, **190**, 263–271.

Adjadj, É., Quiniou, É., Mispelter, J., Favaudon, V. and Lhoste, J.M. (1992a) *Eur. J. Biochem.*, **203**, 505–511.

Adjadj, É., Quiniou, É., Mispelter, J., Favaudon, V. and Lhoste, J.M. (1992b) *Biochimie*, **74**, 853–858.

Arvidsson, K., Jarvet, J., Allard, P. and Ehrenberg, A. (1994) *J. Biomol. NMR*, **4**, 653–672.

Barbato, G., Ikura, M., Kay, L.E., Pastor, R.W. and Bax, A. (1992) *Biochemistry*, **31**, 5269–5278.

Berglund, H., Kovacs, H., Dahlman-Wright, K., Gustafsson, J.A. and Härd, T. (1992) *Biochemistry*, **31**, 12001–12011.

Blackledge, M.L., Brüshweiler, R., Griesinger, C., Schmidt, J.M., Xu, P. and Ernst, R.R. (1993) *Biochemistry*, **32**, 10960–10974.

Cantor, C.R. and Schimmel, P.R. (1980) *Biophysical Chemistry*, Vol. II, Freeman, New York, NY, pp. 459–463.

Careri, G., Fasella, P. and Gratton, E. (1975) *CRC Crit. Rev. Biochem.*, **3**, 141–164.

Cheng, J.W., Lepre, C.A., Chambers, S.P., Fulghum, J.R., Thomson, J.A. and Moore, J.M. (1993) *Biochemistry*, **32**, 9000–9010.

Clore, G.M., Szabo, A., Bax, A., Kay, L.E., Driscoll, P.C. and Gronenborn, A.M. (1990a) *J. Am. Chem. Soc.*, **112**, 4989–4991.

Clore, G.M., Driscoll, P.C., Wingfield, P.T. and Gronenborn, A.M. (1990b) *Biochemistry*, **29**, 7387–7401.

Constantine, K.L., Friedrichs, M.S., Goldfarb, V., Jeffrey, P.D., Sheriff, S. and Mueller, L. (1993) *Proteins*, **15**, 290–311.

Daragan, V.A., Kloczewiak, M.A. and Mayo, K.H. (1993) *Biochemistry*, **32**, 10580–10590.

Dellwo, M.J. and Wand, A.J. (1989) *J. Am. Chem. Soc.*, **111**, 4571–4578.

Deverell, C., Morgan, R.E. and Strange, J.H. (1970) *Mol. Phys.*, **18**, 553–559.

Farrow, N.A., Muhandiram, R., Singer, A.U., Pascal, S.M., Kay, C.M., Gish, G., Shoelson, S.E., Pawson, T., Forman-Kay, J.D. and Kay, L.E. (1994) *Biochemistry*, **33**, 5984–6003.

Favaudon, V. (1983) *Biochimie*, **65**, 593–607.

Frauenfelder, H., Sligar, S.G. and Wolynes, P.G. (1991) *Science*, **254**, 1598–1603.

Fushman, D., Weisemann, R., Thüring, H. and Rüterjans, H. (1994) *J. Biomol. NMR*, **4**, 61–78.

Grasberger, B.L., Gronenborn, A.M. and Clore, G.M. (1993) *J. Mol. Biol.*, **230**, 364–372.

Jones, D.N.M., Searles, M.A., Shaw, G.L., Churchill, M.E.A., Ner, S.S., Keeler, J., Travers, A.A. and Neuhaus, D. (1994) *Structure*, **2**, 609–627.

Kappen, L.S., Napier, M.A. and Goldberg, I.H. (1980) *Proc. Natl. Acad. Sci. USA*, **77**, 1970–1974.

Karplus, M. (1986) *Methods Enzymol.*, **131**, 283–307.

Kay, L.E., Jue, T.L., Bangerter, B. and Demou, P.C. (1987) *J. Magn. Reson.*, **73**, 558–564.

Kay, L.E., Torchia, D.A. and Bax, A. (1989) *Biochemistry*, **28**, 8972–8979.

Kay, L.E., Nicholson, L.K., Delaglio, F., Bax, A. and Torchia, D.A. (1992) *J. Magn. Reson.*, **97**, 359–375.

Kelsh, P.L., Ellena, J.F. and Cafiso, D.S. (1992) *Biochemistry*, **31**, 5136–5144.

Kemple, M.D., Yuan, P., Nollet, K.E., Fuchs, J.A., Silav, N. and Prendergast, F.G. (1994) *Biophys. J.*, **66**, 2111–2126.

Kim, K.-H., Kwon, B.-M., Myers, A.G. and Rees, D.C. (1993) *Science*, **262**, 1042–1045.

Kraulis, P.J. (1991) *J. Appl. Crystallogr.*, **24**, 946–950.

Lefèvre, C., Adjadj, É., Quiniou, É. and Mispelter, J. (1994) *J. Biomol. NMR*, **4**, 689–702.

Lepre, C.A., Cheng, J.-W. and Morre, J.M. (1993) *J. Am. Chem. Soc.*, **115**, 4929–4930.

Lipari, G. and Szabo, A. (1982) *J. Am. Chem. Soc.*, **104**, 4546–4570.

London, R.E. (1989) *Methods Enzymol.*, **176**, 358–375.

McCammon, J.A. and Harvey, S.C. (1987) *Dynamics of Proteins and Nucleic Acids*, Cambridge University Press, Cambridge.

Nicholson, L.K., Kay, L.E., Baldisseri, D.M., Arango, J., Young, P.E., Bax, A. and Torchia, D.A. (1992) *Biochemistry*, **31**, 5253–5263.

Nirmala, N.R. and Wagner, G. (1988) *J. Am. Chem. Soc.*, **110**, 7557–7558.

Nirmala, N.R. and Wagner, G. (1989) *J. Magn. Reson.*, **82**, 659–661.

Orekhov, V.Y., Pervushin, K.V. and Arseniev, A.S. (1994) *Eur. J. Biochem.*, **219**, 887–896.

Palmer III, A.G., Rance, M. and Wright, P.E. (1991) *J. Am. Chem. Soc.*, **113**, 4371–4380.

Palmer III, A.G., Skelton, N.J., Chazin, W.J., Wright, P.E. and Rance, M. (1992) *Mol. Phys.*, **75**, 699–711.

Palmer III, A.G., Hochstrasser, R.A., Millar, D.P., Rance, M. and Wright, P.E. (1993) *J. Am. Chem. Soc.*, **115**, 6333–6345.

Peng, J.W., Thanabal, V. and Wagner, G. (1991) *J. Magn. Reson.*, **95**, 421–427.

Peng, J.W. and Wagner, G. (1992a) *J. Magn. Reson.*, **98**, 308–332.

Peng, J.W. and Wagner, G. (1992b) *Biochemistry*, **31**, 8571–8586.

Powers, R., Clore, G.M., Stahl, S.J., Wingfield, P.T. and Gronenborn, A. (1992) *Biochemistry*, **31**, 9150–9157.

Press, W.H., Flannery, B.P., Teukolsky, S.A. and Vetterling, W.T. (1986) *Numerical Recipes*, Cambridge University Press, Cambridge.

Redfield, C., Boyd, J., Smith, L.J., Smith, R.A.G. and Dobson, C.M. (1992) *Biochemistry*, **31**, 10431–10437.

Ribeiro, A.A., King, R., Restivo, C. and Jardetzky, O. (1980) *J. Am. Chem. Soc.*, **102**, 4040–4051.

Ringe, D. and Petsko, G.A. (1985) *Prog. Biophys. Mol. Biol.*, **45**, 197–235.

Schulz, G.E. and Schirmer, R.H. (1978) In *Springer Advanced Texts in Chemistry*, Vol. 1 (Ed., Cantor, C.R.) Springer, New York, NY, pp. 233–251.

Shaka, A.J., Keeler, J., Frenkiel, T. and Freeman, R. (1983) *J. Magn. Reson.*, **52**, 335–338.

Sklenář, V., Torchia, D. and Bax, A. (1987) *J. Magn. Reson.*, **73**, 375–379.

Solomon, I. (1955) *Phys. Rev.*, **99**, 559–565.

Stone, M.J., Fairbrother, W.J., Palmer III, A.G., Reizer, J., Saier, M.H. and Wright, P.E. (1992) *Biochemistry*, **31**, 4394–4406.

Stone, M.J., Chandrasekhar, K., Holmgren, A., Wright, P.E. and Dyson, H.J. (1993) *Biochemistry*, **32**, 426–435.

Szyperski, T., Luginbühl, P., Otting, G., Güntert, P. and Wüthrich, K. (1993) *J. Biomol. NMR*, **3**, 151–164.

Takashima, H., Amiya, S. and Tobayashi, Y. (1991) *J. Biochem.*, **109**, 807–810.

Teplyakov, A., Obmolova, G., Wilson, K. and Kuromizu, K. (1993) *Eur. J. Biochem.*, **213**, 737–741.

Van Mierlo, C.P.M., Darby, N.J., Keeler, J., Neuhaus, D. and Creighton, T.E. (1993) *J. Mol. Biol.*, **229**, 1125–1146.

Wagner, G. and Wüthrich, K. (1986) *Methods Enzymol.*, **131**, 307–326.

Wagner, G. (1993) *Curr. Opin. Struct. Biol.*, **3**, 748–754.